Wide Angle, Polarization Independent Metamaterial Absorber Unit-Cell for RCS Reduction and Energy Harvesting Applications

Said Choukri, Hakim Takhedmit, Otman El Mrabet, Mariem Aznabet, Laurent Cirio

Wide Angle, Polarization Independent Metamaterial Absorber Unit-Cell for RCS Reduction and Energy Harvesting Applications

Said CHOUKRI[1,2*], Hakim TAKHEDMIT[1], Otman EL MRABET[2], Mariem AZNABET[2], and Laurent CIRIO[1]

[1] Univ Gustave Eiffel CNRS, ESYCOM F-77454 Marne-la-Vallée, France
[2]EMG Group, LaSiT Laboratory, Faculty of sciences, Abdelmalek Essaadi University, Tetouan Maroc
*corresponding author, E-mail: said.choukri@univ-eiffel.fr

Abstract

In this paper, a new design of Metamaterial Absorber unit-cell is presented with a high absorption coefficient of 99.78% at $10\,\mathrm{GHz}$. The numerical results show that the proposed unit-cell has constant performances regardless the polarization state of the incoming waves, a wide angle of absorption up to 70° for TE polarized waves, and 80° for TM, RHCP, LHCP polarized waves is achieved. Analytical circuit model has been developed to describe the matching process between the unit-cell and free space impedances. The monostatic RCS capability of 12×12 metasurface array has been proved numerically by full wave simulation showing more than 10 dB RCS reduction at normal and oblique incidences. Finally a metasurface array was fabricated and tested experimentally, the simulated and measured results are in good agreement in terms of absorption rate and bandwidth, expect a frequency shift in terms of resonance frequency.

Keywords: Metamaterials, Metamaterials Perfect Absorbers, Energy Harvesting, Monostatic RCS, Polarizations

1. Introduction

Electromagnetic absorbing materials, or Radar Absorbing Materials (RAM), were created both in the USA and in Germany during the Second World War [1]. An ideal absorber looks like an effective paint or coating for all polarizations over a wide frequency band and a wide range of incidences. Such material does not exist in reality and it seems difficult to have a prototype that perfectly meets this definition. The applications of absorbers mainly come from the field of Electromagnetic Compatibility (EMC) and Radar discretization [2].

In 2002, N. Engheta showed in a theoretical article [3] that if a surface with metamaterials is placed near a perfectly conductive foil, in a certain frequency band, this structure can behaves like a flat plate with a high impedance on its upper part. Thus, if a resistive sheet is placed on this plate of high impedance, it is possible to obtain a thin structure equivalent to an electromagnetic wave absorber which has reduced dimensions. Several types of electromagnetic wave absorbers have been proposed in the literature, in particular: Dielectric absorbers [4], Structural absorbers with impedance matching [5], Resonant absorbers [6], Magnetic absorbers [7] and Metamaterial absorbers [8]. In [8], the first Printed Circuit Board (PCB) topology of a Metamaterial Perfect Absorber (MPA) unit-cell at microwave frequencies has been introduced. This thin structure, with the thickness of $\lambda_0/35$, has been optimized to achieve an intrinsic impedance close to free space characteristic impedance, hence a near unity absorption rate. This kind of MPA are being utilized for several applications ranging from microwaves to optics and photonics, such as RCS reduction [9], energy harvesting [10]-[11], Radio Frequency Identification (RFID) systems [12], sensing [13], mutual coupling reduction in antenna arrays [14] and so on. Although the functionality of MPA for various applications, harvesting electromagnetic energy and RCS reduction are the best suitable applications with MPA's operating principle, since they capture efficiently the up-coming electromagnetic waves on their front side, then the energy transported may either dissipated or collected depending on the desired application. For RCS reduction by using MPA, the incoming energy will be dissipated inside the unit-cell, since there will be no reflection neither transmission occurs due to the matching process between the unit-cell and the free space impedance, hence the backscattered energy is weaker and the target will be undetectable for certain angle of incidence and certain frequencies. So, in this case a substrate with high loss tangent is highly recommended in the design of the unit-cell. On the other hand, if we aim to use the MPA for energy harvesting purposes, we will have to use a substrate material with low loss tangent and high permittivity in the design of the MPA unit-cell, this will allow us to maximize absorption rate of incident waves and reduce energy dissipation in the cell. Using metamaterial absorbers for energy harvesting and RCS reduction has been explored much during last decade with much appreciable performances notably in terms of high absorption coefficient, wide range of incidence angle, polarization diversity and bandwidth. In [10] M. Dinh proposed a dual-polarized metamaterial absorber cell with double integrated rectifying circuits, the cell operates at $3.75\,\mathrm{GHz}$ and shows a high RF-AC efficiency of 94% that preserved under a wide incident angle

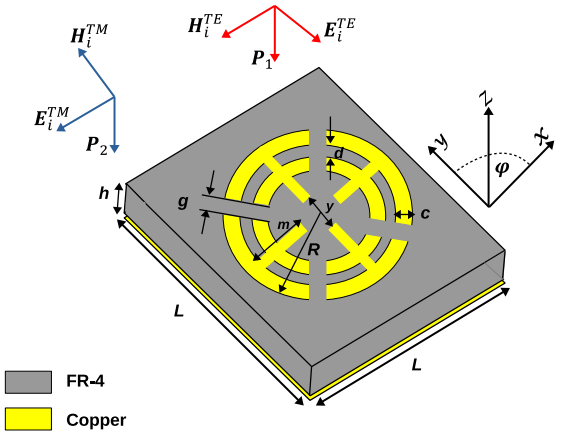

Figure 1: Unit-cell geometry 3D-Design

up to 65° in TE mode and 75° in TM mode. In [15] Long Li *el al.* present a Dual-Band rectifying metasurface with wide range of incidence up to 60° and with considerable conversion efficiency at the operating frequencies.
In this paper, a new design of metamaterial absorber unit-cell is proposed, the unit-cell performs as a perfect absorber with near unity absorption within the frequency bandwidth, which could be a good condidate to harvest surronding electromagnetic waves with different polarizations.

2. The proposed MPA Unit-cell Design

Figure 1 illustrates the proposed design of the metamaterial perfect absorcber structure. The proposed unit-cell consists of two simple concentric metallic rings etched in the center of a square shaped FR-4 substrate with a dielectric constante (ε_r) 4.3 and loss tangent $(\tan\delta)$ 0.025 . Four gaps have been incorporated with the two concentric rings to improve the absorption bandwidth, four strips have also been merged with the two rings in order to make the cell rotationally symmetrical around its z axis, due to this symmetry purpose the cell will be able to capture efficientlly diffrent polarized up-coming waves either circularly or linearly polarized ones. The structure is backed by a full coppered reflective ground plane with the thichness of 35 µm. The geometrical parameters of the unit-cell are listed in table 1. Also shown in figure 1, the external excitation consiste of two incident plane waves propagating from top to bottom with electric feld polarized linearly in the y and x directions respectively for TE and TM modes. $\vec{P}_1$ and $\vec{P}_2$ are the propagation vectors for TE and TM polarized waves respectively.

3. Numerical Studies

3.1. Unit-Cell electromagnetic simulation

The unit-cell was simulated using commercial Computer Simulation Technology (CST) MWS software. The structure was placed in the center of a rectangular square aperture waveguide, boundary conditions are set to be *unit-cell* in the x and y direction, where *open (add space)* boundary was applied in $-z$ and $+z$ directions. Such boundary conditions are suitable for analyzing 2D periodic structures. Then, floquet modal analysis has been performed from waveguide ports to get scattering parameters of the unit-cell. The scattering parameters can be expressed with respect to the co-polarized and cross-polarized components by :

$$S_{11}(\omega) = S_{11}^{xx}(\omega) + S_{11}^{xy}(\omega) \quad (1)$$

$$S_{21}(\omega) = S_{21}^{xx}(\omega) + S_{21}^{xy}(\omega) \quad (2)$$

In equations (1) and (2), the co- and cross-polarized components are denoted by "xx" and "xy", respectively. This configuration holds for an incident electric field polarized in the x direction (TM mode), for the second configuration where the incident electric field vector is polarized in the y direction (TE mode) the co- and cross-polarized components are denoted by "yy" and "yx", respectively. Since the unit-cell presents a low cross-polarization $(S_{11}^{xy} \approx 0)$ and $(S_{21}^{xy} \approx 0)$, the absorption coefficient can be formulated as follows :

$$A(\omega,\theta,\varphi) = 1 - |S_{11}(\omega,\theta,\varphi)|^2 - |S_{21}(\omega,\theta,\varphi)|^2 \quad (3)$$

Since the unit-cell is backed by a full reflective metallic sheet which has the copper thickness of 35 µm, this value remains greater than the skin depth of copper over all the

Table 1: Summary of Unit-Cell geometry.

Parameter	size [mm]
R	6
c	0.6
d	0.4
m	4.4
y	2
g	1.4
h	0.8
L	13

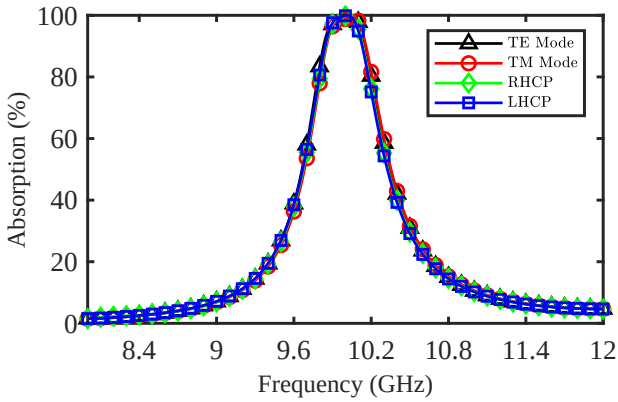

Figure 2: Absorption coefficient versus the frequency for different polarizations of the incident waves : TE, TM, RHCP and LHCP

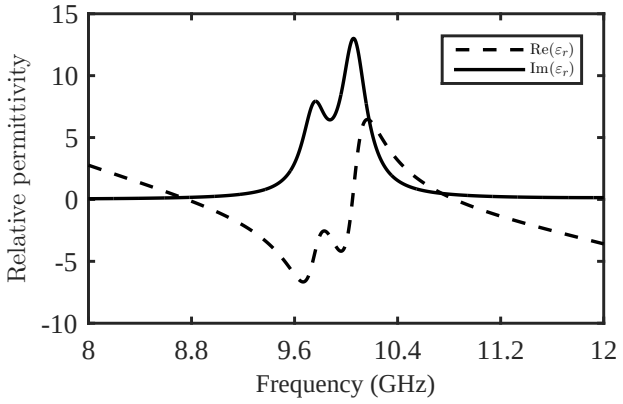

(a)

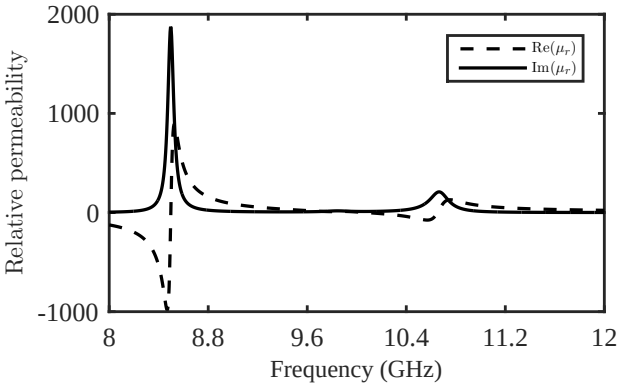

(b)

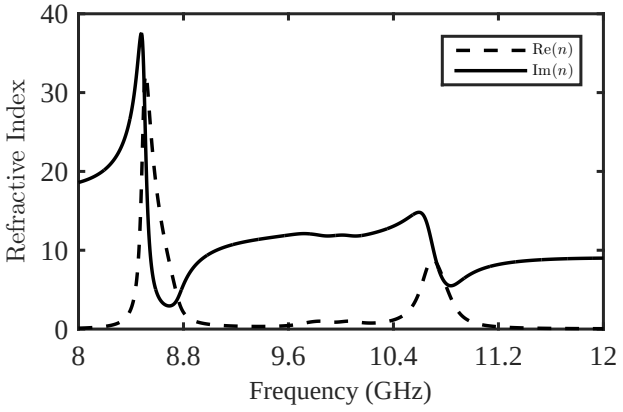

(c)

Figure 3: Metamaterial unit-cell constitutive parameters.

frequency range, so this metallic plane will efficiently prevent incident wave propagation in the other side, resulting zero transmission $S_{21} = 0$ and equation (3) can be reduced to the following form :

$$A(\omega, \theta, \varphi) = 1 - |S_{11}(\omega, \theta, \varphi)|^2 \tag{4}$$

From euqation (4), it is clearly shown that the absorption coefficient depends on the incidence angle (θ) which also known as *Elevation* and on the *Azimuthal* angle φ. Figure 2 sketches the variation of the absorption coefficient computed by using equation (4) under normal incidence ($\theta = 0°$ and $\varphi = 0°$). The unit-cell has been excited with differents polarization states of the incident electric field including linear polarizations TE and TM, as well as circular polarizations RH and LH. We can observe from figure 2 that the response of the unit-cell is very less sensitive to the polarization of the incident waves which proves that the unit-cell can capture and absorbe efficiently all incident waves. Moreover, this feature has an advantage for applications that aim to harvest surronding electromagnetic energy or Radar applications in which the target must not to be detectable by Radar screens. In addition, an absorption bandwidth of $530\,\mathrm{MHz}$ is achieved with an absorption rate above 70%. Figure 3 shows the unit-cell constitutive parameters in real and imaginary parts as a function of frequency in the X-band. The relative permittivity, relative permeability and refractive index are computed using NRW modified reflection only algorithm (RO) and the three parameters are given by following equations :

$$\varepsilon_r(\omega) = 1 + \chi_e(\omega) = 1 + \frac{2j}{k_0(\omega)h}\left(\frac{1 - S_{11}(\omega)}{1 + S_{11}(\omega)}\right) \tag{5}$$

$$\mu_r(\omega) = 1 + \chi_m(\omega) = 1 + \frac{2j}{k_0(\omega)h}\left(\frac{1 + S_{11}(\omega)}{1 - S_{11}(\omega)}\right) \tag{6}$$

$$n(\omega) = \sqrt{\varepsilon_r(\omega)\mu_r(\omega)} \tag{7}$$

Where χ_e and χ_m are respectively the complex electric and magnetic susceptibilities, ω is the angular frequency, k_0 is the free-space wavenumber and h is thickness of the substrate. To achieve the minimum reflection from the absorber unit-cell, the normalized effective impedance (with respect to the free space impedance $Z_0 = 377\ \Omega$) $z_{eff} = \sqrt{\mu_r(\omega)/\varepsilon_r(\omega)}$ needs to be matched with the free space impedance, so that $z_{eff} \approx 1$ at the resonance frequency. From figures 3(a) and 3(b) at $10.04\,\mathrm{GHz}$, $z_{eff} \approx 0.96 - j0.1$ which still acceptable for ensuring good matching. The refcative index can be also formulated by $n(\omega) = n^{'} + jn^{''}$, $n^{'}$ is the refractive index whereas $n^{''}$ is the extinction index, this later compute the losses in the medium. Moreover from figure 3(c), we can see that within the operating frequency band the real part of n is near to zero while the imaginary part has higher values due to the use of FR4 substrte having high loss tangent.

3.2. Equivalent Circuit Model Approach

In order to give a comprehensive understanding of the impedance matching process between the MPA unit-cell and the free space, we propose an analytical circuit model which is based on circuit theory and transmission line theory. The unit-cell with its three parts (Reflective metallic sheet, Substrate and the resonator) is described by the equivalent circuit shown in figure 4, whose parameters have been rigorously calculated and optimized. Moreover, the metal plane which plays the role of a reflector is modeled by its complex impedance based on the approximation of good conductor, this impedance is given by [16]:

$$Z_m = (1 + j)\sqrt{\frac{\omega\mu}{2\sigma}} = (1 + j)\frac{1}{\sigma\delta_m(\omega)} \tag{9}$$

$$Z_{in}(\omega) = \frac{A_1(\omega)\left(1-\omega^2 LC\right) - A_2(\omega)C\omega + j\left[1 - LC\omega^2 + A_1(\omega)C\omega\right]}{A_3(\omega)\left(1 - LC\omega^2 - RC\omega\right) + A_1(\omega) - RC\omega A_2(\omega) + j\left[2A_2(\omega) - LCA_2(\omega)\omega^2\right]} \quad (8)$$

$$A_1(\omega) = -\frac{Z_c}{\sigma\delta_m(\omega)}\tan\left(\beta_s(\omega)h\right) \qquad A_2(\omega) = Z_c\tan\left(\beta_s(\omega)h\right) \qquad A_3(\omega) = \frac{1}{\delta_m(\omega)}$$

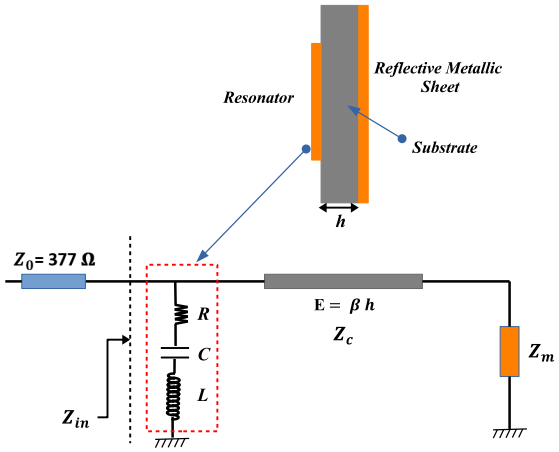

Figure 4: Equivalent circuit model of the unit-cell

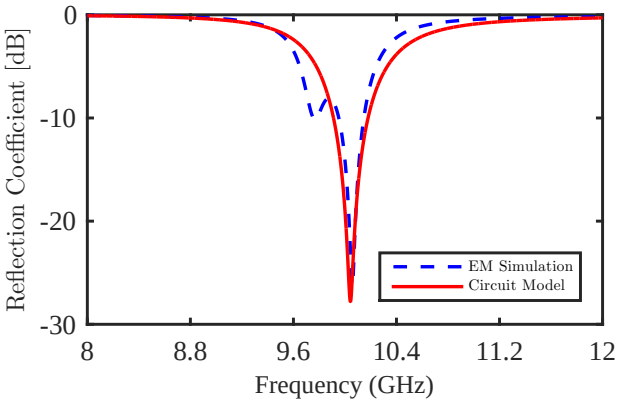

Figure 5: Unit-Cell reflection coefficient : EM Simulation versus circuit model responses

Where ω is the angular frequency, μ is the permeability, σ is the copper conductivity and δ_m is the skin depth of the metal. Then, based on tansmission lines theory, the substrate is modeled by a transmission line of length h terminated by a short circuit to take into account the ground connection. The input impedance seen looking into the line is deduced by an equivalence between fields theory and circuit theory and it is given by the following equation :

$$Z_s(\omega) = j\sqrt{\frac{\mu_{rs}\mu_0}{\varepsilon_{rs}\varepsilon_0}}\tan\left(\beta_s h\right) = jZ_c\tan\left(\beta_s(\omega)h\right) \quad (10)$$

Where $\beta_s = \beta_0/\sqrt{\varepsilon_r\mu_r}$ is propagation constant in the substrate, ε_{rs} and μ_{rs} are the constitutive parameters of the substrate material while Z_c its characteristic impedance. The etched metallic resonator on the top side of the substrate, which is the fundamental element that controls the cell's resonance, is modeled by a series RLC resonant tank which has the following impedance :

$$Z_r(\omega) = R + jL\omega + \frac{1}{jC\omega} \quad (11)$$

Since, the equivalent impedance seen looking into the input port of the circuit is calculated by equation (8). the three unknowns circuit parameters R, L and C are calculated by solving the following equation :

$$Z_{in}(\omega)|_{\omega=\omega_r} = Z_0 \quad (12)$$

Where $\omega_r = 2\pi f_r$ is the resonance frequency. After solving equation (12), the values of R, L and C are found to be respectively $R = 601.62\ m\Omega$, $L = 2.54\ pH$ and $C = 1.06\ pF$. Figure 5 shows the frequency response of the circuit model compared to electromagnetic simulation

3.3. Effect of Incident and Azimuthal Angles on the Absorption of the MPA unit-cell

In this section, we study numerically the effects of changing the incident and azimuthal angles of the incident electromagnetic waves on the unit-cell performances. MPA structures normally exhibit high absorption rate in normal incidence, but when increasing the incident angle θ the absorption values decrease automatically due to the nonlinearity between the reflection coefficient and the incident angle, which is given by equations (13) and (14) for TE and TM modes, respectively :

$$\Gamma^{TE}(\theta) = \frac{\cos\left(\theta\right) - \sqrt{n^2 - \sin^2\left(\theta\right)}}{\cos\left(\theta\right) + \sqrt{n^2 - \sin^2\left(\theta\right)}} \quad (13)$$

$$\Gamma^{TM}(\theta) = \frac{-n^2\cos\left(\theta\right) - \sqrt{n^2 - \sin^2\left(\theta\right)}}{n^2\cos\left(\theta\right) + \sqrt{n^2 - \sin^2\left(\theta\right)}} \quad (14)$$

Where n is the refractive index of the MPA structure and θ is the incident angle. Since the challenge in designing MPA structures is to achieve a high absorption coefficient for large incident angles. Figure 6 depicts the absorption spectra of the unit-cell in which the variation of absorption coefficient is reported as a function of the incident and azimuthal angles. Note that when sweeping theta or phi angle the other angle is fixed at 0°. From figure 6(a) for TE mode, we note that the unit-cell shows a less sensitive response to the variation of the angle θ, and the performance is still surprisingly quasi-uniform up-to 70°, which we denote by θ_{max}. As the angle is varied away from this

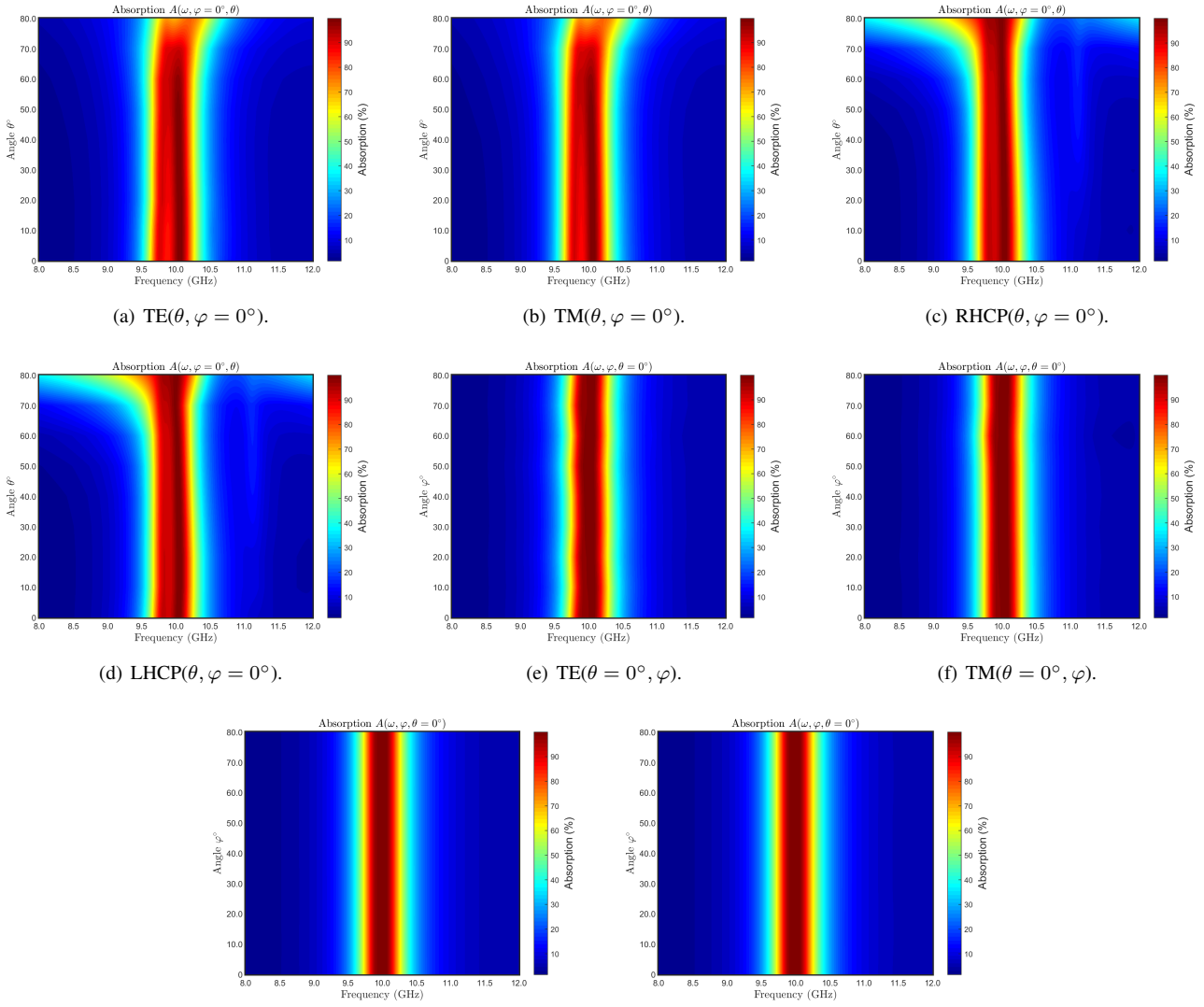

(a) TE($\theta, \varphi = 0°$). (b) TM($\theta, \varphi = 0°$). (c) RHCP($\theta, \varphi = 0°$).

(d) LHCP($\theta, \varphi = 0°$). (e) TE($\theta = 0°, \varphi$). (f) TM($\theta = 0°, \varphi$).

(g) RHCP($\theta = 0°, \varphi$). (h) LHCP($\theta = 0°, \varphi$).

Figure 6: Absorption Spectra of the unit-cell for different polarizations : Elevation angle θ test : (a)-Mode TE,(b)-Mode TM,(c)-RHCP and (d)-LHCP. Azhimutal angle φ test (e)-Mode TE, (f)-Mode TM, (g)-RHCP and (h)-LHCP.

value ($\theta_{max} = 70°$), the absorption rate becomes less than 70% practically for the whole spectral badwidth. From figures 6(b), 6(c) and 6(d) similar effects, but with the value $\theta_{max} = 80°$ of theta, have been observed when exciting the uni-cell with TM modes. The signification of the maximum value of theta lies in how large the angle of incidence the unit-cell can support for the absorption of the incoming electromagnetic wave. So, all the electromagnetic waves arriving with an angle of incidence whose value is included within the aperture angle θ_{max} of the absorber cone will be captured efficiently by the unit-cell with the minimum reflection as explained in figure 7. This structure has been designed to be rotationally symetrical around its z axis, this fact is clearly observed in figures 6(e), 6(f), 6(g) and 6(h) where the response is insensitive to the variation of φ, respectively for TE,TM, RHCP and LHCP polarizations and the unit-cell exhibits a constant absorption coefficient.

4. Metasurface RCS Reduction Capability

In this section, a demonstration of the metasurface RCS reduction capability is given with respect to the incidence angle at the maximum absorbance frequency point. The metasurface is built by arranging 12×12 unit-cell in two dimensions. At normal incidence, the RCS reduction by a metasurface consisting with $M \times N$ unit-cells is expressed as [9] :

$$RCSR_{normal} = 20 \log \left| \sum_{m=1}^{M} \sum_{n=1}^{N} E_{mn} e^{ik_0 \beta_{mn}} \right| \quad (15)$$

Where E_{mn} and β_{mn} are respectively the amplitude and phase of the reflected electric field of the cell in row m and colum n of the metasurface, and k is the wavenumber of the incident wave in free-space. By using equation 8, we can easily obtain the RCS reduction trough substituting

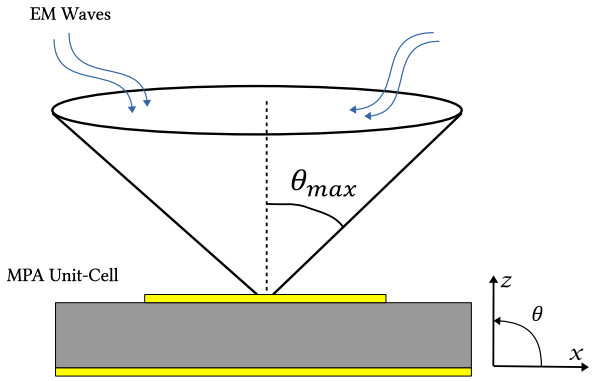

Figure 7: Unit-cell maximum width angle

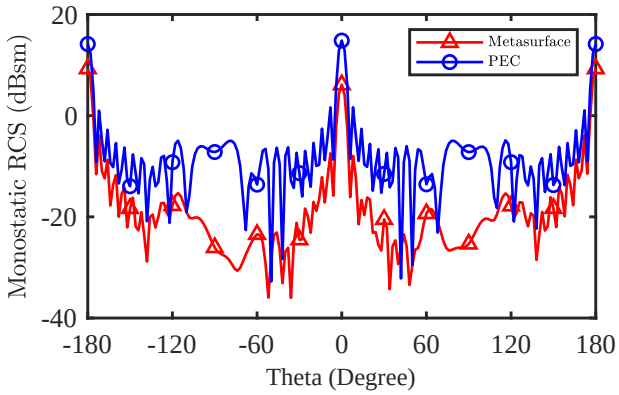

Figure 8: Monostatic RCS versus the elevation angle θ of the metasurface and equal-sized PEC at 10 GHz

the amplitude and phase of the reflected electric field by the unit-cell. For an oblique incidence at angles θ and φ the RCS reduction is given by the following equation :

$$RCSR_{oblique} = 20\log\left|\frac{E(\theta,\varphi)}{E_i}\right| \tag{16}$$

Where E_i is the magnitude of the incident electric field vector, and $E(\theta,\varphi)$ is the reflected back electric field by the whole metasurface array cells which can be expressed by :

$$E(\theta,\varphi) = \sum_{m=1}^{M}\sum_{n=1}^{N} E_{mn} e^{ik_0[(m-1)d_x\cos\varphi + (n-1)d_y\sin\varphi]\sin\theta} \tag{17}$$

The monostatic RCS of the metasurface has been computed numericaly using HFSS, where excitation with plane waves in spherical coordinates was used to illuminate the metasurface array at the frequency of interest (10 GHz). In order to test the RCS reduction for different values of the incidence angle, we sweeped the angle θ from $-180°$ to $+180°$ while the angle φ was fxed at $0°$. Then the same simulation setup has been performed to compute the monostatic RCS of equal-sized PEC sheet to the metasurface and results are shown in figure 8. We can see clearly that the metasurface contributes to reduce the monostatic RCS in all the range of θ where the RCS reduction reached 10 dB or more at normal incidence.

Figure 9: Fabricated metasurface array (12×12) cells

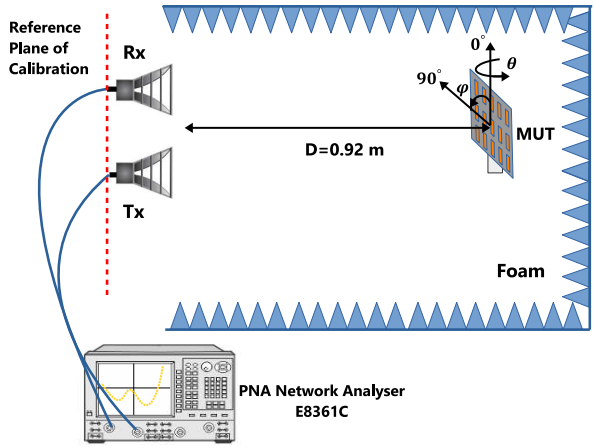

Figure 10: Free-space measurement setup

5. Experimental results

In order to evaluate the performances of the metamaterial absorber unit-cell and verify its performances, we fabricated a square prototype of 144 unit-cells. Figure 9 shows the fabricated sample on FR4 epoxy substrate with total dimensions of $15.3 \times 15.3 \times 0.08\ cm^3$. Figure 10 describes the measurement setup used to evaluate the absorption coefficient in the free-space. Accordingly, two X-Band horn antennas were used to transmit electromagnetic waves and receive the reflected signal from the metasurface, an Agilent Power Network Analyser (PNA) is used to excite the transmitter and measure the S-parameters of the sample. The far-fleld distance was fixed at $0.92\ m$. The measurement setting can be summarized as follow : first the reflection coefficient from a conductive plat, which has the same dimensions of the sample, was extracted through the measured scattering parameter (S_{21}), then the metalic plat was replaced by the metasurface absorber which its reflection coefficient was extracted also through measured transmission coefficient (S_{21}). The final reflection coefficient of the metasurface was calculated through the substraction of the two measured reflection coefficients. Finally, The ab-

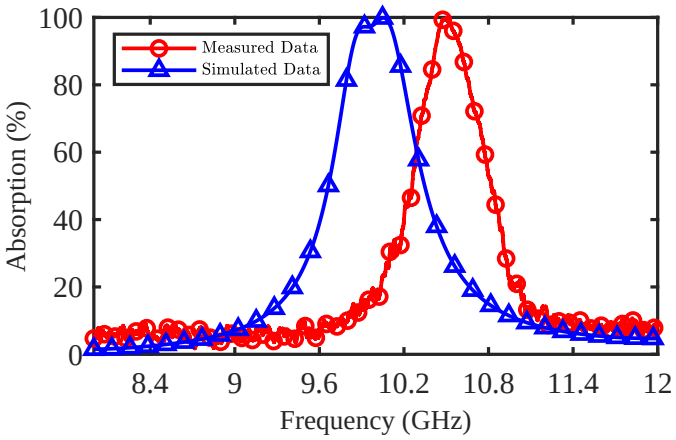

Figure 11: Simulated and measured absorption coefficient at normal incidence

sorption coefficient was calculated by using equation 4 assuming normal incidence and measured results are reported in figure 11. The measured results are in good agreement with numerical results in terms of the absorption rate and the absorption bandwidth, except that a frequency shift was observed between the two results. This discrepancy is probably due to the manufacturing tolerances and the measurement setup imperfections.

6. conclusion

In this work, a metamaterial absorber unit-cell has been designed and simulated numericaly and the obtained results showed that the absorption is above 70% within the frequency bandwidth of 560 MHz, the unit-cell has the capability to absorb elecctromagnetic waves with different polarizations. A circuit model has been developed providing physical insights into the matching process with the free-space characteristic impedance to achieve full absorption. The monostatic RCS reduction of the metasurface array has been proved with 10 dB and more reduction at normal and oblique incidences. The absorption coefficient of a (12×12) metasurface array was calculated experimentally under normal incidence which has a near unit absorption rate at 10.45 GHz.

Acknowledgement

This work was carried out within the framework of TOUBKAL PROJECT : TBK/20/100 Campus N° 43761TJ under the Franco-Moroccan cooperation between CNRST and Campus France.
Authors would like to thank Stephane PROTAT for his technical support in the prototypes fabrication and measurements.

References

[1] P. SAVILLE, Review of Radar Absorbing Materials, *Defence R&D Canada -Atlantic,PO Box 012,Dartmouth, NS,CA,B2Y 3Z7* , Canada, 2005.

[2] P.A Zhukov and V.Yu Kirillov, The application of radar absorbing materials to reduce interference emissions from instruments and devices of spacecraft electrical systems, *18th International Conference "Aviation and Cosmonautics" (AviaSpace-2019)*, IOP Publishing, New York, 2019.

[3] N.Engheta, Thin absorbing screens using metamaterial surfaces, *Antennas and Propagation Society International Symposium*, IEEE,Vol 2 pp.392-395, 2002.

[4] S. Capaccioli, M. Lucchesi, P. A. Rolla,et al, Dielectric response analysis of a conducting polymer dominated by the hopping charge transport, *Journal of Physics: Condensed Matter*, vol. 10, no 25, p. 5595, 1998.

[5] A. Fallahi, A. Enayati, Modeling Pyramidal Absorbers Using the Fourier Modal Method and the Mode Matching Technique, *IEEE Transactions on Electromagnetic Compatibility*, vol. 58, Issue: 3, p. 6, 2016.

[6] K. Naishadham, P.K. Kadaba, Measurement of the microwave conductivity of a polymeric material with potential applications in absorbers and shielding, *IEEE Transactions on Microwave Theory and Techniques*, vol. 39, Issue: 7, p. 89, 1991.

[7] S. Sugimoto,S. Kondo,K. Okayama,H. Nakamura,D. Book,T. Kagotani,M. Homma,H. Ota, M. Kimura, R. Sato, M-type ferrite composite as a microwave absorber with wide bandwidth in the GHz range, *IEEE Transactions on Magnetics*, vol. 35, Issue: 5, p. 154, 1999.

[8] N. I Landy *et al.*, Perfect metamaterial absorber, *Physical Review Letters, APS*, vol. 100, no. 4, p. 207-402, 2008.

[9] Z. Zhang *el Al et al.*, Broadband RCS Reduction by a Quaternionic Metasurface, *Materials MDPI*, vol. 14, p. 2787, 2021.

[10] M. Dinh, N. Ha-Van, N. T. Tung, M. Thuy Le, Dual-Polarized Wide-Angle Energy Harvester for Self-Powered IoT Devices, *IEEE Access*, vol. 9, no. 2, 2021.

[11] S. CHOUKRI, H. TAKHEDMIT, O. EL MRABET, L. CRIO, Energy Harvesting using loaded Metamaterial Absorber Unit-Cell with polarization independent Capability, *JNRSE, Grenoble, FRANEC*, 2021.

[12] Y. Okano, S. Ogino, K. Ishikawa, Development of Optically Transparent Ultrathin Microwave Absorber for Ultrahigh-Frequency RF Identification System, *IEEE Transactions on Microwave Theory and Techniques*, vol. 60, Issue: 60, p. 70, 2012.

[13] M. L. Hakim, *et Al.*, Polarization insensitive symmetrical structured double negative (DNG) metamaterial absorber for Ku-band sensing applications, *Scientific Reports*, vol. 12, no. 479, 2022.

[14] J. Zhang, J. Li, J. Chen, Mutual Coupling Reduction of a Circularly Polarized Four-Element Antenna Array Using Metamaterial Absorber for Unmanned Vehicles, *IEEE Access*, vol. 7, P. 13, 2019.

[15] L. Li, X. Zhang, C. Song, W. Zhang, T. Jia, Y. Huang, Compact Dual-Band, Wide-Angle, Polarization- Angle -Independent Rectifying Metasurface for Ambient Energy Harvesting and Wireless Power Transfer, *IEEE Transactions on Microwave Theory and Techniques*, vol. 69, Issue. 3, P. 20, 2021.

[16] David M. Pozar, Microwave Engineering, *Wiley Publishing*, Fourth Edition, 2011.

[17] Ruey-Bing Hwang, Periodic Structures: Mode-Matching Approach and Applications in Electromagnetic Engineering, *Wiley Publishing*, First Edition, 2013.